# Microbial Pyrolysis for the Sustainable Synthesis of Nanoparticle-Embedded Carbon Electrocatalysts

**Authors:** Tali Dotan[1], Yoo Kyung Go[1], Maximiliano J. Fornerod[1], Megan E. Núñez[2], Jesus M. Lopez Baltazar[1], Grace I. Anderson[1], Ariel L. Furst[1*]

[1] Department of Chemical Engineering, Massachusetts Institute of Technology, Cambridge, MA, 02139, United States

[2] Department of Chemistry and Program in Biochemistry, Wellesley College, Wellesley, Massachusetts

*To whom correspondence should be addressed: afurst@mit.edu | ORCID: https://orcid.org/0000-0001-9583-9703

## Abstract

Electrocatalytic processes are essential for a sustainable global economy, yet conventional catalyst synthesis often relies on hazardous reagents and insulating binders that impede performance. Here, microbial extracellular electron transfer for nanoparticle synthesis is integrated with the controlled pyrolysis of microbial monolayers to generate nanoparticle-embedded carbon electrodes. Surface immobilization of *Shewanella oneidensis* using DNA "Velcro" yields uniform single-microbe-thick layers that are readily patterned and converted into conductive, turbostratic carbon films at temperatures between 800 °C and 1,100 °C. These bio-derived films exhibit progressive graphitic ordering and reach a minimum sheet resistance of 1.49 kΩ/sq, approaching the performance of pyrolyzed synthetic photoresists. Moreover, by leveraging the intrinsic biosynthetic capabilities of *S. oneidensis*, 3-5 nm palladium nanoparticles are formed directly on the cell surface and seamlessly integrated into the carbon matrix upon pyrolysis. These composites reduce the hydrogen evolution reaction overpotential by 100 mV. This bottom-up bioengineering approach is anticipated to enable the sustainable, programmable fabrication of next-generation electrocatalysts for diverse energy conversion applications.

## 1. Introduction

Catalytic processes are essential to support the current global economy, with critical materials ranging from plastics to antibiotics dependent on these chemical transformations. However, most industrial-scale approaches require high temperatures and pressures achieved through the burning of fossil fuels, rendering them unsustainable and inefficient. In contrast, electrocatalysis is easily integrated with renewable energy inputs and isgenerally conducted at ambient temperatures and pressures[1]. The expansion of such approaches offers a sustainable alternative to conventional thermocatalysis, decreasing our reliance on fossil fuels while supporting diverse chemical transformations[2,3].

Nanoparticle (NP)-based electrocatalysts are prevalent because they connect molecular-level control of active sites with macroscopic device-scale performance. Their small size yields a

high surface area-to-volume ratio, ensuring thata large fraction of active sitesare exposed at surfaces, edges, and defects where electrochemical reactions occur[4],Supporting high current densities at relatively low metal loadings. In addition, nanoparticle composition, crystal structure, and morphology can be tuned to optimize the binding energies of key intermediates, modulate reaction pathways, and improve selectivity for a broad range of electrocatalytic reactions, including hydrogen evolution (HER), oxygen reduction (ORR) and evolution (ORE), $CO_2$ reduction ($CO_2$RR), and small-molecule oxidation[5,6]. Taken together, these advantages make nanoparticle catalysts an attractive and versatile platform for designing efficient, tailored electrocatalysis systemsacross diverse chemistries. However, current approaches to synthesis introduce significant constraints onthe realization of these. Many conventional synthetic routes rely on strong chemical reducing agents, organic solvents, and surface-active ligands or surfactants to control nucleation and growth, stabilize ultrasmall particles, and prevent aggregation[4]. These reagents can be toxic, environmentally hazardous, and difficult to handle at scale. Surfactants and capping agents that are essential for size and shape control often passivate catalytically active surfaces and must be removed in a separate treatment step, which frequently involves high-temperature annealing or harsh chemical washes. Such post-treatments can cause sintering and growth of particles, destroying desited nanoscale features[5]. As a result, there is a persistent gap between the ideal of precisely engineered nanoparticle catalysts and the realities of practical, scalable synthesis.

An alternative approach to nanoparticle synthesis that circumvents many of the challenges with current methods is NP biosynthesis. Of particular interest is the application of microbes with unique respiratory or metabolic capabilities for the generation of NPs. One key pathway that has been efficiently exploited for such reactions is extracellular electron transfer (EET), which allows microbes to exchange electrons directly with their environment. As model systems for such NP production, *Shewanella spp.* are easy to work with, and many species are genetically tractable[7]. In fact, *Shewanella* spp. have been used to generate both NPs and composite materials[7]. As an example, *S. algae* generated 5 nm diameter platinum (Pt) NPs in the periplasm using $PtCl_6^{2-}$ ions in under an hour at ambient temperature and physiological pH with lactate as an electron donor[8]. Additionally, *S. oneidensis* has been used to generate palladium[9–11] and Pd-Pt alloy NPs[12]. Overall, a strong capability of *Shewanella spp.*, for eco-friendly NP synthesis has been established. Nevertheless, a further layer of complexity arises when these nanoparticles are integrated into functional electrodes, where overall electrocatalytic performance depends critically on the architecture and interfaces of the catalyst-support-electrolyte system, not simply on the intrinsic activity of the NPs. Generally, nanoparticle powders are dispersed with polymeric binders to form inks that are cast onto conductive substrates such as carbon cloth, carbon paper, metal foils, or foams. While this approach is simple and widely used, it introduces several fundamental limitations: polymer binders are typically electronically insulating and can obstruct active sites, increase charge-transfer and film resistance, and impede ion transport through the catalyst layer[13,1,2]. Nanoparticles in such composite films often aggregate during ink preparation, drying, or operation, further decreasing

the effective active surface area. Mechanical adhesion between the catalyst layer and the underlying current collector can be poor, particularly under gas-evolving or high-current conditions, leading to cracking, delamination, or loss of active material over time[14]. Even in more advanced, binder-free electrodes where nanoparticles or nanostructured catalysts are grown directly on supports, the electronic and structural integration is often imperfect. Catalysts may decorate only the outer surfaces of fibers or the top layer of a foam, leaving internal pores and transport pathways underutilized. Electrical contact between nanoparticles and the conductive scaffold can be heterogeneous, producing local regions of high resistance and nonuniform current distribution. At the same time, the porous architecture must support efficient ion diffusion and rapid release of product gases. If pore structure, wettability, and surface topography are not well controlled, gas bubbles or concentration gradients can build up within the electrode, masking the intrinsic benefits of the nanocatalyst[1]. These interfacial and architectural challenges can render much of the potential performance of nanoparticle catalysts \lost at the level of electrode design.

Together, these challenges highlight is the importance of growing interest in new strategies that incorporate the co-design of catalyst synthesis and electrode architecture, rather than treating them as isolated steps. Approaches that form nanoparticles *in situ* on or within a conductive scaffold, under mild conditions and without insulating binders, offer a way to simultaneously address synthetic, interfacial, and transport limitations[1,15]. Here, we present a unified strategy that bridges living-material patterning with microfabrication by co-designing catalyst synthesis, support formation, and spatial architecture in a single bottom-up process. By enforcing single-cell 2D spatial arrangement using DNA 'Velcro' tethering prior to pyrolysis, we transform *Shewanella oneidensis* monolayers into conductive, uniform carbon thin films (~1-2 μm thickness, sheet resistance 1.49 kΩ/sq) that mimic pyrolyzed synthetic photoresists. Crucially, when coupled with in situ extracellular reduction of palladium, the biogenic cell membrane serves as a sacrificial template that spatially confines 3-5 nm Pd nanoparticles during high-temperature pyrolysis (1,000 °C), preventing thermal sintering without requiring synthetic surfactants or capping agents. The resulting 2D composite yields a binder-free electrocatalyst where low precious-metal loadings achieve a 100 mV reduction in hydrogen evolution reaction (HER) overpotential. By overcoming the fundamental transport, interfacial, and structural limitations of conventional bulk microbial carbonization, this work establishes a programmable platform for patterned carbon micro-architectures and cost-effective, high-efficiency electrocatalysts.

## 2. Results and Discussion

### 2.1 DNA-Directed Microbial Monolayers on Fused Silica

Pyrolysis of synthetic photoresists such as SU-8 has been developed as an approach to generate patterned turbostratic carbon materials on inert substrates. These materials are conductive, chemically robust, and can be controlled at the microscale through photolithographic patterning of the resist prior to pyrolysis[5,17–19] (Figure 1a). In theory, microbes can support the generation

of similar materials when their placement on a substrate is tightly controlled. However, in the absence of control over their deposition, dense biofilms that are tens of microns thick are generated, which can lead to inconsistent characteristics following pyrolysis. In contrast, single microbe deep monolayersensure consistent and reproducible coverage andarchitecture across diverse substrates. This precision makes such layers an attractive starting point for the development of high-performance interfaces.

We have developed a simple approach to control the deposition of microbes at electrodes through their immobilization as a single layer using DNA as "Velcro"[20,21]. When a surface is modified with a short, synthetic single-stranded DNA (ssDNA) sequence and the cell surface is modified with the complement, hybridization between the complementary sequences capture of the microbes at the surface (Figure 1b). Consistent and dense microbial films are generated with this approach that are only a single microbe thick (1-2 microns). Further, the control afforded by DNA immobilization enables patterning on substrates. Analogous to photoresist patterning, "Velcro" patterning was used to define surface structures via selective DNA attachment by blocking non-target ("negative") areas. To explicitly demonstrate this spatial definition across macro-scale features, orthogonal ssDNA sequences end-labeled with 6-FAM (green) and Cy5 (red) were selectively spotted onto distinct circular domains (~4 mm diameter) on the fused silica substrate (Figure 1b, inset). Fluorescence imaging confirms sharp boundaries between adjacent spots with minimal non-specific cross-adsorption in masked background areas. Because cell capture is strictly mediated by sequence-specific hybridization, this spatial pre-patterning of the DNA template dictates the downstream 2D arrangement of the microbial monolayer, offering a direct, programmable strategy to define patterned carbon micro-architectures upon pyrolysis without requiring conventional photoresists.

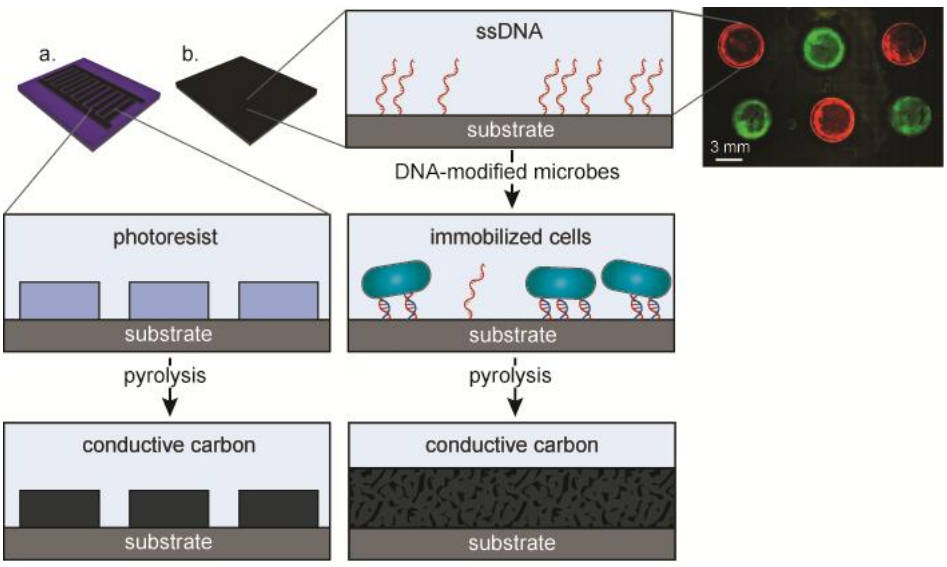



**Figure 1. Comparison of carbonated films pyrolysis.** (a) Schematic of conventional SU-8 photoresist patterning and pyrolysis to yield patterned conductive carbon microstructures on a substrate. (b) Conceptual illustration of DNA-directed microbial monolayer assembly and pyrolysis. Surface modification with single-stranded DNA (ssDNA) "Velcro" enables

sequence-specific spatial immobilization (*top-right inset:* fluorescence image demonstrating spatially defined patterning of 6-FAM- (green) and Cy5-labeled (red) ssDNA spot arrays on fused silica; scale bar: 3 mm). Subsequent hybridization with complementary DNA-functionalized *Shewanella oneidensis* cells yields a single-microbe-thick layer, which transforms upon high-temperature pyrolysis into a continuous, conductive carbon thin film.

Because of its stability at high temperatures, fused silica glass was used as a substrate for the DNA "Velcro"[22,23]. To modify the glass with ssDNA, the substrate was initially modified via silanization with (3-Aminopropyl)triethoxysilane (APTES), resulting in the display of an amine. Subsequent reaction with glutaraldehyde yielded a carboxylic acid that is readily coupled to amine-modified ssDNA (Figure 2a). Similarly, cells were modified with complementary ssDNA using an established protocol involving initial oxidation of outer-membrane polysaccharides with periodate, followed by aniline-catalyzed hydrazone formation with hydrazide-functionalized oligonucleotides[21]. This modification approach maintains microbial viability while enabling chemical modification of cells with ssDNA (Figure 2b).
Following modification of both cells and fused silica with ssDNA, cells were incubated at the glass surface to allow the DNA to hybridize. The conditions for monolayer formation were optimized for surface density through variation of the incubation time and solution density of cells, with subsequent Live/Dead staining using SYTO 9 and propidium iodide (PI). SYTO 9 permeates all cells, while PI is excluded by cells with intact membranes and penetrates only compromised membranes. Image segmentation of the live cells (green fluorescence) reveals a uniform surface coverage of ~39.6% across the substrate (Figure 2c). Red fluorescent signals are sparse and are evenly distributed, showing that dead cells are not found in clusters (Figure 2d).

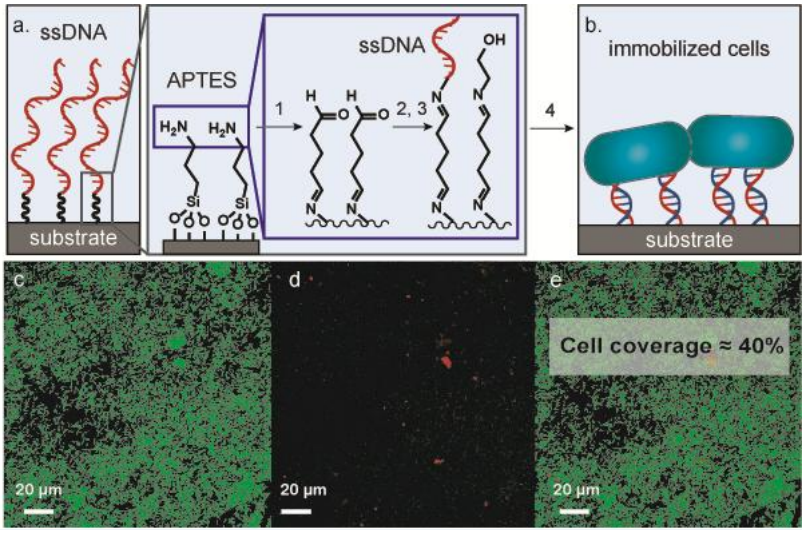



**Figure 2. DNA-"Velcro" strategy for generating *S. oneidensis* microbial monolayers on glass.** (a) Scheme of fused silica surface modification: plasma-cleaned glass is silanized with APTES to introduce surface amines, crosslinked with glutaraldehyde, and

subsequently coupled to amine-modified C2 ssDNA, followed by blocking of remaining aldehyde end groups with ethanolamine and reduction to form a stable DNA-terminated substrate. (b) Scheme of cell-surface DNA conjugation: *S. oneidensis* are functionalized through DNA-i linker complementary to surface-bound ssDNA. (c,d,e) Confocal imaging of *S. oneidensis* cells attached to fused silica with live/dead stain, using SYTO 9 (c, green) and propidium iodide (PI) (d, red), and overlay (e).

## 2.2 Temperature-Dependent Property Changes in *Shewanella*-Derived Carbonaceous Material

Carbon materials exhibit highly diverse morphological and electronic properties. Native bacterial biomass constitutes non-conductive carbon dominated by $sp^3$-hybridized structures (single C-C, C-O, and C-N bonds in proteins, lipids, and polysaccharides) with high heteroatom content (~12-15% O, N, H) that disrupts electron transport[24]. These isolated molecular domains (amino acid chains, sugar polymers, and nucleotide fragments) lack extended π-conjugation, yielding resistivities $>10^6$ Ω·cm and confining electrons to individual molecules. In contrast, more ordered conductive carbon such as glassy carbon features turbostratic $sp^2$ graphene sheets with delocalized π-electrons spanning micrometers across continuous 3D networks, minimal heteroatom content (<5%), and sheet resistances of ~1 kΩ/sq[25,26]. This state exhibits moderate graphitic ordering and a nanocrystalline turbostratic structure with randomly rotated graphene layers, which can be characterized by spectroscopic and thermal analysis techniques[24,27].

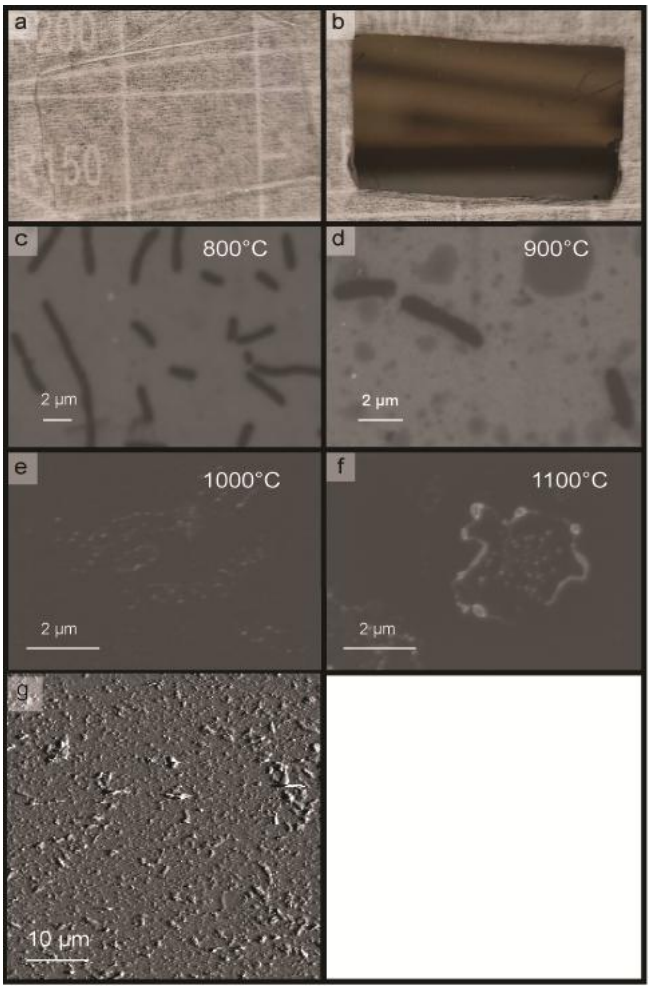



**Figure 3. Temperature-dependent morphological evolution of Shewanella-derived carbon films during pyrolysis.** Photographs of DNA-"Velcro"-patterned *S. oneidensis* films on fused silica before (a) and after (b) pyrolysis at 1,100 °C. SEM images of DNA-attached films pyrolyzed at 800 °C-1,100 °C (c-f), revealing recognizable temperature-dependent morphology from cell-shaped features to irregular embedded contours of the original cells remaining. (g) AFM surface topography image showing partially embedded bacterial film with uniform coverage across the monolayer pyrolyzed at 1000 °C.

Pyrolysis was utilized as a means to modulate the chemical composition and electrical characteristics of the bacterial film. A high vacuum condition of 200 mTorr or below was found to be essential for promoting material crystallization and preventing carbon combustion arising from exothermic oxidation reactions with residual air. Under a controlled thermal profile with a constant heating rate of 5 °C $min^{-1}$, the maximum temperature, maintained within the range of 700 °C to 1,100 °C, served as the primary parameter governing the resulting material properties. Pyrolysis of the *Shewanella* biofilms was found to induce strong, temperature-dependent changes in morphology, structure, and electrical transport. Bacterial films that initially appeared transparent on glass were transformed into a highly reflective, mirror-like coating at the highest pyrolysis temperatures, with intermediate temperatures yielding dark, opaque layers at the highest pyrolysis temperature, while similar layers with only DNA

assembly on the surface did not produce any visual changes upon pyrolysis (Figure 3a-b). To relate these macroscopic visual changes to underlying microstructural evolution, the films were first examined by scanning electron microscopy (SEM). SEM imaging showed that these visual changes were accompanied by marked microstructural evolution: untreated DNA-"Velcro"-attached cells exhibit typical rod-like morphologies of approximately 1-2 μm in length, whereas films pyrolyzed at 800 °C and 900 °C were observed with recognizable cell-shaped features embedded within a continuous carbonized matrix (Figure 3c-d). At 1,000 °C, only faint outlines of the original cellular shapes were visible, and at 1,100 °C the residue was reduced to irregular embedded contours, consistent with extensive high-temperature reorganization of cellular components and possible phase transitions in membrane-derived material (Figure 3e-f). Collectively, these visual and microscopic observations demonstrate that coalescence of the biogenic material into a continuous carbon film occurred with increasing maximum pyrolysis temperature.

To further evaluate surface topography and film continuity across larger spatial dimensions, atomic force microscopy (AFM) was conducted on a pyrolyzed film at 1,000 °C (Figure 3g). The AFM analysis confirms a continuous coating with uniform coverage across tens of micrometers, where the cellular contours are partially embedded at the surface, maintaining individual cell morphologies.

The observed micro-morphological changes reflect transformations in the carbon microstructure, corresponding to the formation of conductive and electroactive films. Thermogravimetric analysis (TGA) was performed to identify the dominant temperature range for weight loss associated with dense material formation. The TGA was carried out on dried *S. oneidensis* MR-1 pellets under inert nitrogen over a temperature range from room temperature to 1,400 °C at a rate of 10 °C $min^{-1}$ (Figure 4a in yellow). An initial mass loss of 7.01% was observed between room temperature and 200 °C, with a maximum weight-loss rate of 0.07% $°C^{-1}$ near 104 °C, consistent with removal of residual water. Then, a dominant decomposition event occurred between 200-600 °C (55.19% mass loss), consistent with active pyrolysis of biological systems[28–30]. A further analysis of this mass loss through the derivative TGA curve (Figure 4a in orange) resolved a primary peak at 308 °C (>0.5% $°C^{-1}$), assigned to rapid volatilization of readily decomposable components (peptidoglycans, lipids), and a peak at the 400-600 °C region that reflected a breakdown of recalcitrant macromolecules and initial carbon aromatization, leaving a stable carbon-rich framework[30]. Above 600 °C, a secondary, slower mass loss of 13.31% was detected, peaking at 880 °C. At this stage, most readily decomposable organics had already been decomposed, and the remaining material is a mineral-containing char. This gradual, smaller mass loss of the high-temperature regime was interpreted as reflecting continued carbonization and devolatilization of the char, together with thermal transformations of mineral phases such as carbonates, phosphates, and metal oxides associated with *Shewanella* cells[31,32]. This behavior was found to mirror reports on glassy-carbon

formation, in which slow, high-temperature structural reorganization is typically observed, rather than discrete additional decomposition steps[27].

To further interrogate these high-temperature transitions and their relationship to the final graphitic ordering, differential scanning calorimetry (DSC) was employed on dried *Shewanella* MR-1 cells (Figure 4b). The DSC trace displayed a broad endothermic feature centered around 1,100 °C, with no sharp phase-transition peaks. This broad minimum was consistent with the substantial energy input required for aromatization, densification, and progressive elimination of heteroatoms (C-H, C-O, C-N) from the residual char over a wide temperature range[33,34]. When considered together, the TGA and DSC data were found to corroborate the hypothesis that increasing pyrolysis temperature drives a transition from hydrated, polymer-rich biomass to a more ordered, turbostratic carbon framework.

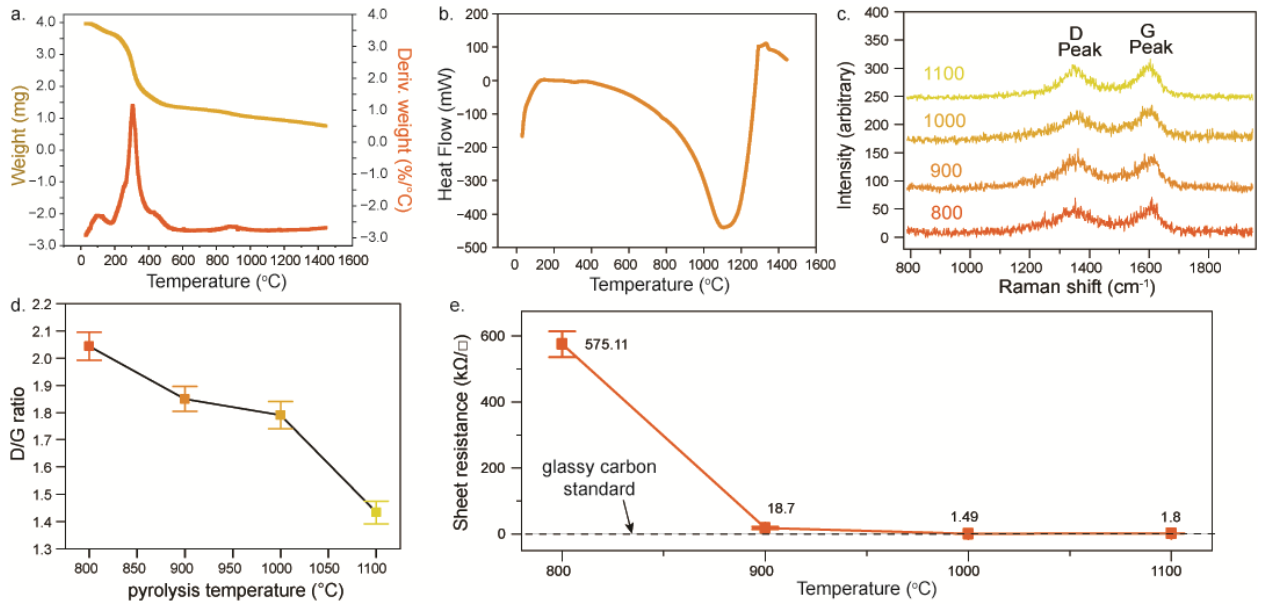



**Figure 4. Thermal, structural, and electrical characterization of pyrolyzed Shewanella films.** (a) Thermogravimetric analysis (TGA) and derivative TGA of dried *S. oneidensis* MR-1 biomass under nitrogen at 10 °C/min. (b) Differential scanning calorimetry (DSC) trace of dried cells. (c) Raman spectra of films pyrolyzed at 800, 900, 1,000, and 1,100 °C, showing D (graphite-like, ~1,350 $cm^{-1}$) and G (amorphic, ~1,600 $cm^{-1}$) bands indicative of carbon. (d) D/G peak area ratio as a function of maximum pyrolysis temperature, decreasing monotonically. (e) Sheet resistance of pyrolyzed films measured by four-point probe.

## 2.3 Spectroscopic and Electronic Characteristics of the Pyrolyzed Material

To translate the observations into quantitative metrics of carbon ordering, the films were subsequently probed by Raman spectroscopy. In the thin carbon structures featuring turbostratic $sp^2$ graphene sheets with delocalized π-electrons in continuous 3D networks alongside

amorphous $sp^3$-hybridized carbon, a high G-band fraction is desired to optimize conductive and catalytic properties[35,36]. Raman spectroscopy of the pyrolyzed films confirmed the formation of graphitic carbon and revealed a systematic improvement in structural ordering with temperature. Replicate films on glass were pyrolyzed at maximum temperatures of 800 °C, 900 °C, 1,000 °C, and 1,100 °C, and Raman spectra were collected at three distinct locations on each sample to assess in-plane uniformity (Figure 4c). Across all conditions, spectra exhibiting the two characteristic first-order bands of graphitic carbon were obtained: a D band near 1,350 $cm^{-1}$ (associated with lattice defects and disorder in $sp^2$ carbon, prominent in amorphous carbon) and a G band near 1,600 $cm^{-1}$ (corresponding to in-plane vibrations of $sp^2$-bonded carbon atoms in graphite-like domains)[24]. Because no other carbon-containing components apart from *S. oneidensis* were present (and DNA at negligible amounts), the appearance of these features was taken to indicate that the bacterial biomass had been converted into a carbonized film during high-temperature treatment. Quantitative analysis of peak areas showed that the D/G intensity ratio decreased monotonically with increasing pyrolysis temperature, with the largest drop observed between 1,000 °C and 1,100 °C (Figure 4d). This trend was interpreted as signifying a progressive reduction in structural disorder and an increase in graphitic ordering within the carbon network at higher temperatures. The evolution of the D/G ratio was found to be consistent with prior reports for biomass-derived carbons, in which this metric is used as a proxy for crystallinity, suggesting that bacterial carbon was polymerized and crystallized in a manner analogous to wood and biochar from plant pyrolysis[25,35].

Electrical characterization was performed to quantify sheet resistance and validate the films' functionality as conductive electrodes. While structural techniques provide insights into morphology, four-point probe measurements assess direct charge transport properties, which are critical for minimizing ohmic losses and ensuring efficient electron transfer to catalytic sites. High conductivity is essential for uniform current distribution across electrode surfaces, thereby maximizing catalyst utilization and enhancing overall electrocatalytic rates (Figure 4e). Films produced at 800 °C exhibited relatively high resistance, which was observed to decrease sharply as the maximum pyrolysis temperature was increased to 900 °C and 1,000 °C, in agreement with the improved graphitic ordering inferred from spectroscopic and thermal analyses. Above 1,000 °C, the sheet resistance reached a plateau and remained essentially unchanged at 1,100 °C, despite independent evidence for continued structural ordering at this highest temperature. The minimum sheet resistance achieved was 1.49 kΩ/sq, a value that approaches reported values for thin glassy carbon films (approximately 1.075 kΩ/sq)[37]. This saturation was taken to suggest that, beyond a certain level of crystallinity, the conductivity is limited not by local ordering but by mesoscale features such as grain boundaries, surface roughness, and inhomogeneous film thickness that impede long-range electron transport. Consistent with reports for pyrolyzed photoresists, in which sheet resistance scales inversely with pyrolysis temperature[5,17–19], these bacterial-derived carbon films were thus positioned within a similar performance regime, while microstructural non-uniformity was identified as a likely lower bound on achievable sheet resistance for these biogenic electrodes.

## 2.4 Biosynthesis of Nanoparticles

As an extracellular electron transfer mechanism, *S. oneidensis* mediates the reduction of $PdCl_4^{2-}$ into crystalline, 3–5 nm palladium nanoparticles localized within the periplasm and outer membrane (Figure 5a,b), aligning with reported biogenic Pd synthesis pathways. After establishing that microbial films can be converted into conductive, turbostratic carbon electrodes, palladium nanoparticles were incorporated to provide catalytic activity and accelerate target electrochemical reactions. *S. oneidensis* used extracellular electron transfer under anaerobic conditions to biosynthesize palladium nanoparticles with diameters of 3-5 nm (Figure 5a,b)[12,41]. To systematically control the spatial density and overall surface loading of noble-metal nanoparticles across the cellular template, the bio-reduction duration was varied while maintaining daily additions of 1 mM $Na_2PdCl_4$ precursor solution. Shortening the biosynthesis incubation time to 2 days yields a sparse, low-coverage distribution of isolated Pd nanoparticles along the outer cell membrane and periplasmic space (Figure 5c, 'Low Pd coverage'). Extending the incubation duration to 8 days with daily precursor replenishment significantly increases particle nucleation density, forming a continuous, highly populated monolayer of Pd nanoparticles without inducing cell lysis or particle aggregation prior to pyrolysis (Figure 5d, 'High Pd coverage'). This fully biotic synthesis approach offers several key advantages over conventional chemical or physical methods. The Pd(0) particles nucleate and grow directly on bacterial cell surfaces via biologically mediated reduction of Pd(II), remaining stably anchored to the biomass scaffold[42]. This surface confinement ensures monodisperse 3-5 nm dimensions and uniform and controlled distribution, which are preserved through pyrolysis into the final carbon matrix, unlike ex situ mixing where nanoparticles readily agglomerate due to high surface energy, leading to loss of active surface area and reduced catalytic efficiency. Moreover, through genetic engineering of microbial electron transfer pathways, nanoparticle size and distribution can be precisely controlled, while stimuli-responsive engineering enables dynamic regulation of biosynthesis in response to environmental triggers. Furthermore, the seamless integration of Pd nanoparticles within a microbially derived carbon matrix retains the material's biological origin, promoting favorable interactions with living cells or biofilms compared to synthetic carbon-Pd composites produced via harsh post-treatments. This biocompatibility is particularly advantageous for bioelectrochemical systems, where electrode-cell interfaces drive performance, or for future sensor or bio-interface applications where a versatile, binder-free template is of interest. Finally, microbial extracellular reduction eliminates the need for toxic chemical reducing agents (e.g., $NaBH_4$, hydrazine) and high-energy inputs common in abiotic syntheses[21], enabling sustainable, room-temperature production of catalytically active nanoparticles without hazardous waste streams. These attributes collectively enable bottom-up fabrication of high-performance, biohybrid electrocatalysts from renewable biomass feedstocks.

## 2.5 Palladium Nanoparticles Integrated Carbon Materials

Nanoparticle-integrated composites were fabricated by following a similar process flow to the carbonated electrodes. Pd nanoparticle-coated cells were immobilized on fused silica using the DNA "Velcro" attachment strategy[21], and pyrolysis at 1,000 °C yielded a composite material in which palladium is embedded within a conductive carbon matrix (Figure 5e-f). The degree of sintering at the different temperatures is still to be studied and evaluated for its catalytic effect. As a proof of concept, the catalytic activity of the resulting films was evaluated at one specific pyrolysis temperature, for the hydrogen evolution reaction (HER) in 0.5 M sulfuric acid. Catalytic activity refers to the ability of the embedded Pd nanoparticles to accelerate electrochemical reaction kinetics by lowering the overpotential, and as a result, lowering the required reaction energy inputs. A three-electrode configuration was employed, with a platinum wire as the counter electrode and an Ag/AgCl reference electrode. The overpotential at 10 $mA/cm^2$ was recorded versus Ag/AgCl and converted to the RHE scale. Across three independent measurements, the Pd-decorated carbon film exhibited an overpotential of 520 mV, compared to 620 mV for the bare carbon film. Although lower overpotentials have been reported for other palladium nanoparticle systems[12], the 100 mV reduction in overpotential was reached with only partial nanoparticle coverage as shown in the TEM (Figure 5a-b). It is therefore expected that increasing the metal loading would provide an even larger energetic benefit. The degree of sintering at the different temperatures is still to be studied and evaluated for its catalytic effect. This proof-of-concept demonstration highlights the high potential of this platform and opens significant space for further research into the optimization of nanoparticle stability within biogenic carbon matrices. The observed electrocatalytic performance highlights the unique architectural advantages of co-pyrolyzing spatially controlled 2D microbial monolayers over standard catalyst-ink or bulk-pyrolysis methodologies. In conventional noble-metal electrocatalysts, precious-metal cost remains a primary barrier to industrial scale; catalyst powders buried within thick, binder-bound porous layers are electronically insulated or inaccessible to the electrolyte, leading to poor atomic utilization. In contrast, our DNA-directed 2D thin-film configuration ensures that biosynthesized 3-5 nm Pd nanoparticles remain uniformly dispersed and directly anchored at the conductive carbon surface. This open, binder-free 2D architecture exposes virtually all active sites to the electrolyte while facilitating rapid interfacial charge transport and unhindered release of evolved $H_2$ gas bubbles during HER. Consequently, significant overpotential reductions (~100 mV) are realized at remarkably low metal loadings. Furthermore, because the cell membrane acts as an intrinsic physical scaffold during carbonization, the need for chemical reducing agents or surfactant ligands, which typically passivate active catalytic sites and require harsh post-treatments, is entirely circumvented.

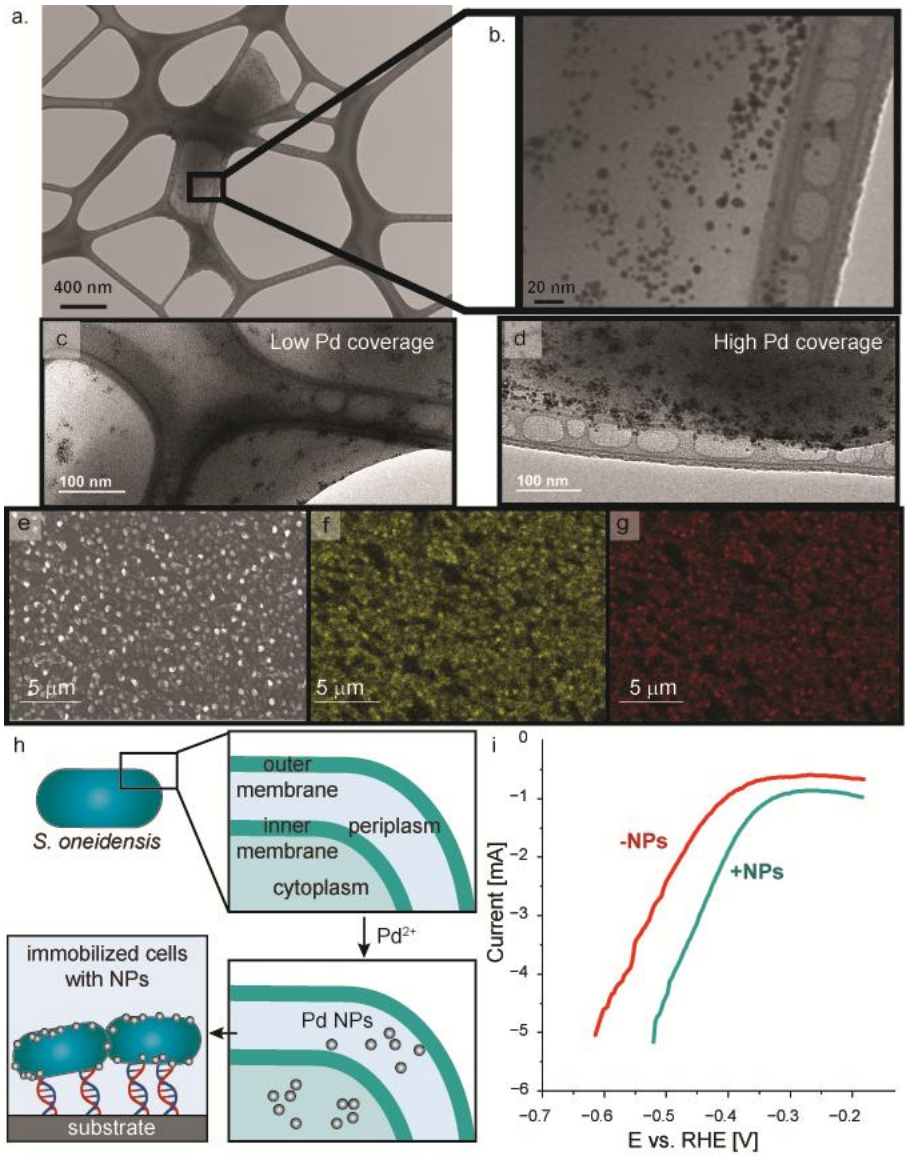



**Figure 5. Biosynthesized palladium nanoparticles (NPs) and their integration into carbon electrodes for proof-of-concept HER.** (a, b) High-resolution TEM image of biosynthesized Pd nanoparticles anchored to the *Shewanella* cell surface. (c, d) TEM images demonstrating density control with daily 1 mM $Na_2PdCl_4$ additions: (c) low Pd coverage after 2 days, and (d) high Pd coverage after 8 days. EDX analysis (e, f) and SEM image (g) of Pd-decorated *Shewanella* films on fused silica after DNA-"Velcro" attachment and pyrolysis at 1,000 °C. (h) Schematic overview of NP biosynthesis and subsequent cellular immobilization. (i) HER polarization curves in 0.5 M $H_2SO_4$ for bare and Pd-decorated *Shewanella* films in a three-electrode configuration.

## 3. Conclusions

Efficient, scalable electrocatalysis requires electrode materials that are not only highly active and conductive but also sustainable in both their composition and fabrication. In this work, we demonstrate that DNA-“Velcro”-patterned *Shewanella oneidensis* MR-1 can be converted by

pyrolysis into turbostratic carbon films. Crucially, the DNA 'Velcro' tethering mechanism enables sequence-specific spatial control over cell assembly, allowing for the programmable 2D patterning of carbon micro-architectures prior to pyrolysis without relying on conventional photoresists. We show that the maximum pyrolysis temperature governs the transformation of this biological template into a carbon film across structural, thermal, and electronic metrics. With increasing temperature from 800 to 1,100 °C, SEM imaging reveals a progression from clearly discernible cell shapes embedded in carbon to a nearly featureless, coalesced coating, while Raman spectra report a monotonic decrease in the D/G intensity ratio, indicating reduced defect density and enhanced graphitic ordering. Complementary TGA and DSC measurements resolve a dominant 200-600 °C mass-loss event associated with primary biomass decomposition and char formation, followed by slower mass loss and a broad endotherm extending to ~1,100 °C attributed to continued aromatization, densification, and heteroatom removal in the emerging carbon framework. These structural and thermal changes coincide with a sharp drop in sheet resistance between 800 and 1,000 °C and a subsequent plateau near 1.5 kΩ/sq at 1,000-1,100 °C, approaching values for thin glassy carbon and suggesting that, beyond this point, mesoscale features rather than local crystallinity limit charge transport. We further show that coupling this platform to microbial Pd nanoparticle biosynthesis yields carbon films in which catalytically active Pd is embedded within the biogenic carbon matrix, reducing the HER overpotential by ~100 mV despite low metal loadings. Because both the cellular scaffold and the nanoparticle phase are biologically produced and the final properties are tunable through simple variations in pyrolysis conditions, this strategy establishes bacterial films as programmable precursors for architected carbon and metal-carbon composite electrodes, and provides a foundation for extending pyrolyzed microbial materials to other redox-active metals, host organisms, and device geometries. Building on this proof-of-concept, tuning the thermal profile offers a straightforward pathway to systematically control nanoparticle sintering dynamics and further maximize catalytic surface area in future device iterations. By eliminating insulating binders, preventing high-temperature nanoparticle sintering without passivating surfactants, and maximizing precious-metal atomic efficiency, this 2D co-pyrolysis strategy addresses core performance bottlenecks in electrocatalytic energy conversion. Looking forward, the soft biogenic origin and precise DNA patternability of these carbonized monolayers also offer a prospective platform for future planar micro-devices and electrochemical sensors.

## 4. Experimental Section

### 4.1 DNA binding to silica surface

100 mm JGS1 UV-grade fused silica wafers (MSE Supplies, 500 µm DSP w/bevel) were diced into 1 cm × 1 cm squares using a dicing saw, sonicated in acetone for 15 min, rinsed with isopropyl alcohol, dried under nitrogen, and plasma-cleaned (high voltage, 15-20 min). Cleaned chips were transferred to a nitrogen-filled glovebox and immersed in a 1:20 (v/v) solution of (3-aminopropyl)triethoxysilane (APTES) in anhydrous toluene for 20 min with gentle agitation,

then washed four times with anhydrous toluene, rinsed in acetone, and dried under vacuum. The amine-terminated surfaces were activated by applying glutaraldehyde (10% v/v in PBS, ~200 µL per substrate) for 7 min, followed by rinsing with PBS/Milli-Q water and drying with compressed air. Amine-modified C2 DNA (full formula is available in the SI) was diluted to 50 µM in RNase-free PBS, and 20 µL was deposited on each activated substrate, covered, and incubated overnight in the dark to form covalently bound DNA monolayers via glutaraldehyde crosslinking. The surfaces were then washed ten times with Milli-Q water and incubated for at least 20 min in a freshly prepared blocking solution (585.2 mg ethanolamine·HCl and 377 mg sodium cyanoborohydride in 50 mL Milli-Q water), followed by three sequential water washes. DNA-functionalized substrates were then stored in RNase-free PBS at 4 °C, yielding a stable DNA-terminated platform for subsequent bacterial attachment.

## 4.2 Bacterial Liquid Culture Preparation

*Shewanella oneidensis* MR-1 was streaked from frozen glycerol stocks onto LB agar plates and grown overnight at 30 °C. A single colony was inoculated into LB media and grown overnight at 30 °C with shaking to reach OD600 ≈ 1.0. Resulting cells were either used directly for DNA "Velcro" attachment to fused silica substrates or first subjected to palladium nanoparticle biosynthesis prior to surface immobilization.

## 4.3 Pd biosynthesis

*S. oneidensis* MR-1 cells were grown overnight aerobically in LB media, then transferred to a vinyl anaerobic chamber (COY Laboratory Products, Grass Lake, MI, USA) maintained at <50 ppm $O_2$ using a 20% $CO_2$/80% $N_2$ gas mix with palladium catalyst. Cells were then inoculated in Shewanella basal medium (SBM) and grown anaerobically for 24 h to reach $OD_{600}$ ≈ 0.1. Cells were pelleted, washed with SBM, and resuspended in Pd growth solution containing 100 µM $Na_2PdCl_4 \cdot 3H_2O$ as previously reported[9]. Biosynthesis proceeded for 6 days under anaerobic conditions, followed by PBS washing. Pd nanoparticle-coated cells were characterized by HR-TEM prior to DNA "Velcro" attachment to fused silica substrates.

## 4.4 Cell-DNA Conjugation ("Velcro" Attachment)

Cells were pelleted and washed twice with PBS. Cells were resuspended in 500 µM sodium periodate ($NaIO_4$) in PBS (500 µL per standard batch) and incubated 15 min at 30 °C with shaking to generate reactive aldehyde groups on cell surface polysaccharides. 1 M glucose was added (10% v/v of periodate volume) to quench excess oxidant, yielding 0.1 M final glucose. Cells were washed twice with PBS, then once with 0.5 M NaCl, 0.1 M MOPS buffer (pH 7.4). Cells were resuspended in NaCl/MOPS containing 20 mM aniline and 30-40 µM M2-i linker DNA (complementary to surface-immobilized C2 strands, formula is available in the SI). Conjugation proceeded via oxime ligation for 18 h (overnight) at room temperature with shaking, protected from light.

### 4.5 Post-Conjugation Processing

Conjugated cells were pelleted, washed to remove unbound DNA and reagents, resuspended in PBS and adjusted to cell concentration of 5-8 $OD_{600}$. Then the cells were drop-casted on the DNA-tethered silica substrates and formed into a "sandwich" structure with glass microscope slides, and reacted for 2 hours. This yields *S. oneidensis* MR-1 monolayers covalently tethered to substrate-bound DNA Velcro, enabling uniform, selective bacterial attachment with controlled surface coverage.

### 4.6 Pyrolysis

Pyrolysis was carried out in an OTF-1500X-8Z eight-zone split-tube furnace (MTI, CA, USA; maximum temperature 1500 °C) using alumina boats. Samples were first heated from room temperature to 50 °C over 10 min, followed by a 2 h hold at 50 °C under vacuum to reach a pressure of 200 mTorr. The temperature was then increased at 5 °C $min^{-1}$ to the selected maximum temperature (800-1,100 °C) and maintained for 1 h. Finally, the furnace was allowed to cool to room temperature under vacuum at a maximum rate of 5 °C $min^{-1}$.

## Supporting Information

Supporting Information is available from the Wiley Online Library or from the author.


## Acknowledgements

This work was supported by funding from the ARO (W911NF2210106) and the MIT Energy Initiative. Electron microscopy was performed at the MIT.nano characterization facilities and the Koch Institute Nanotechnology Materials Core Facility.


## Conflict of Interest

There are no conflicts of interest to declare.

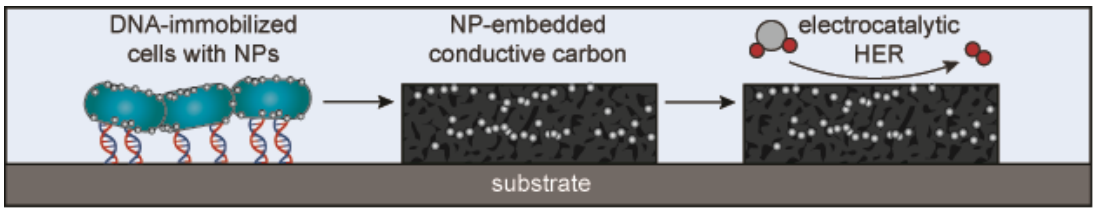
## Data Availability Statement

The data that support the findings of this study are available from the corresponding author upon reasonable request.


## Keywords

Electroactive bacteria, Engineered living materials, Electrode materials, Pyrolysis

## Table of Contents (TOC) / Graphical Abstract Entry




**Process Flow:** DNA-immobilized cells with NPs → NP-embedded conductive carbon → electrocatalytic HER

References

(1) Seh, Z. W.; Kibsgaard, J.; Dickens, C. F.; Chorkendorff, I.; Nørskov, J. K.; Jaramillo, T. F. Combining Theory and Experiment in Electrocatalysis: Insights into Materials Design. *Science* **2017**, *355* (6321), eaad4998. https://doi.org/10.1126/science.aad4998
(2) Wang, G.; Dai, Y.; Yang, H.; Xiong, Q.; Wang, K.; Zhou, J.; Li, Y.; Wang, S. A Review of Recent Advances in Biomass Pyrolysis. *Energy Fuels* **2020**, *34* (12), 15557–15578. https://doi.org/10.1021/acs.energyfuels.0c03107
(3) Francke, R.; Schille, B.; Roemelt, M. Homogeneously Catalyzed Electroreduction of Carbon Dioxide—Methods, Mechanisms, and Catalysts. *Chem. Rev.* **2018**, *118* (9), 4631–4701. https://doi.org/10.1021/acs.chemrev.7b00459
(4) Polshettiwar, V.; Varma, R. S. Green Chemistry by Nano-Catalysis. *Green Chem.* **2010**, *12* (5), 743. https://doi.org/10.1039/b921171c
(5) Kim, J.; Song, X.; Kinoshita, K.; Madou, M.; White, R. Electrochemical Studies of Carbon Films from Pyrolyzed Photoresist. *J. Electrochem. Soc.* **1998**, *145* (7), 2314–2319. https://doi.org/10.1149/1.1838636
(6) Mohan, D.; Pittman, C. U.; Steele, P. H. Pyrolysis of Wood/Biomass for Bio-Oil: A Critical Review. *Energy Fuels* **2006**, *20* (3), 848–889. https://doi.org/10.1021/ef0502397
(7) Rajput, V. D.; Minkina, T.; Kimber, R. L.; Singh, V. K.; Shende, S.; Behal, A.; Sushkova, S.; Mandzhieva, S.; Lloyd, J. R. Insights into the Biosynthesis of Nanoparticles by the Genus *Shewanella*. *Appl. Environ. Microbiol.* **2021**, *87* (22), e01390-21. https://doi.org/10.1128/AEM.01390-21
(8) Konishi, Y.; Ohno, K.; Saitoh, N.; Nomura, T.; Nagamine, S.; Hishida, H.; Takahashi, Y.; Uruga, T. Bioreductive Deposition of Platinum Nanoparticles on the Bacterium Shewanella Algae. *J. Biotechnol.* **2007**, *128* (3), 648–653. https://doi.org/10.1016/j.jbiotec.2006.11.014
(9) Dundas, C. M.; Graham, A. J.; Romanovicz, D. K.; Keitz, B. K. Extracellular Electron Transfer by *Shewanella Oneidensis* Controls Palladium Nanoparticle Phenotype. *ACS Synth. Biol.* **2018**, *7* (12), 2726–2736. https://doi.org/10.1021/acssynbio.8b00218
(10) De Windt, W.; Boon, N.; Van Den Bulcke, J.; Rubberecht, L.; Prata, F.; Mast, J.; Hennebel, T.; Verstraete, W. Biological Control of the Size and Reactivity of Catalytic Pd(0) Produced by Shewanella Oneidensis. *Antonie Van Leeuwenhoek* **2006**, *90* (4), 377–389. https://doi.org/10.1007/s10482-006-9088-4
(11) Cheng, Y.-Y.; Wang, W.-J.; Ding, S.-T.; Zhang, M.-X.; Tang, A.-G.; Zhang, L.; Li, D.-B.; Li, B.-B.; Deng, G.-Z.; Wu, C. Pyruvate Accelerates Palladium Reduction by Regulating Catabolism and the Electron Transfer Pathway in Shewanella Oneidensis. *Appl. Environ. Microbiol.* **2021**, *87* (8), e02716-20. https://doi.org/10.1128/AEM.02716-20

(12) Xu, H.; Xiao, Y.; Xu, M.; Cui, H.; Tan, L.; Feng, N.; Liu, X.; Qiu, G.; Dong, H.; Xie, J. Microbial Synthesis of Pd–Pt Alloy Nanoparticles Using *Shewanella Oneidensis* MR-1 with Enhanced Catalytic Activity for Nitrophenol and Azo Dyes Reduction. *Nanotechnology* **2019**, *30* (6), 065607. https://doi.org/10.1088/1361-6528/aaf2a6
(13) Apfelbeck, F. A. C.; Heger, J. E.; Zheng, T.; Guan, T.; Schwartzkopf, M.; Roth, S. V.; Müller-Buschbaum, P. Influence of the Polymer Binder Composition on the Charge Transfer Resistance, Morphology, and Crystallinity of $LiFePO_4$ Electrodes Revealed by Electrochemical Impedance Spectroscopy and Grazing Incidence Small- and Wide-Angle X-ray Scattering. *Small Sci.* **2024**, 2400154. https://doi.org/10.1002/smsc.202400154
(14) Pollet, B. G. The Use of Ultrasound for the Fabrication of Fuel Cell Materials. *Int. J. Hydrog. Energy* **2010**, *35* (21), 11986–12004. https://doi.org/10.1016/j.ijhydene.2010.08.021
(15) Kosimaningrum, W. E.; Le, T. X. H.; Holade, Y.; Bechelany, M.; Tingry, S.; Buchari, B.; Noviandri, I.; Innocent, C.; Cretin, M. Surfactant- and Binder-Free Hierarchical Platinum Nanoarrays Directly Grown onto a Carbon Felt Electrode for Efficient Electrocatalysis. *ACS Appl. Mater. Interfaces* **2017**, *9* (27), 22476–22489. https://doi.org/10.1021/acsami.7b04651
(16) Al-Rumaihi, A.; Shahbaz, M.; Mckay, G.; Mackey, H.; Al-Ansari, T. A Review of Pyrolysis Technologies and Feedstock: A Blending Approach for Plastic and Biomass towards Optimum Biochar Yield. *Renew. Sustain. Energy Rev.* **2022**, *167*, 112715. https://doi.org/10.1016/j.rser.2022.112715
(17) Pramanick, B.; Vazquez-Pinon, M.; Torres-Castro, A.; Martinez-Chapaa, S. O.; Madou, M. Effect of Pyrolysis Process Parameters on Electrical, Physical, Chemical and Electro-Chemical Properties of SU-8-Derived Carbon Structures Fabricated Using the C-MEMS Process. *Mater. Today Proc.* **2018**, *5* (3), 9669–9682. https://doi.org/10.1016/j.matpr.2017.10.153
(18) Ranganathan, S.; McCreery, R.; Majji, S. M.; Madou, M. Photoresist-Derived Carbon for Microelectromechanical Systems and Electrochemical Applications. *J. Electrochem. Soc.* **2000**, *147* (1), 277. https://doi.org/10.1149/1.1393188
(19) Singh, A.; Jayaram, J.; Madou, M.; Akbar, S. Pyrolysis of Negative Photoresists to Fabricate Carbon Structures for Microelectromechanical Systems and Electrochemical Applications. *J. Electrochem. Soc.* **2002**, *149* (3), E78. https://doi.org/10.1149/1.1436085
(20) Go, Y. K.; Dotan, T.; Kuo, C.-C.; Gut, M.; Furst, A. Understanding Interface-Driven Dynamics of Microbial Carbonate Precipitation through DNA-Driven Tethering. October 30, 2025. https://doi.org/10.26434/chemrxiv-2025-6pdcx
(21) Twite, A. A.; Hsiao, S. C.; Onoe, H.; Mathies, R. A.; Francis, M. B. Direct Attachment of Microbial Organisms to Material Surfaces Through Sequence-Specific DNA Hybridization. *Adv. Mater.* **2012**, *24* (18), 2380–2385. https://doi.org/10.1002/adma.201104336
(22) Souder, W.; Hidnert, P. Measurements on the Thermal Expansion of Fused Silica. *Sci. Pap. Bur. Stand.* **1925**, *21*, 1. https://doi.org/10.6028/nbsscipaper.198
(23) Mader, M.; Schlatter, O.; Heck, B.; Warmbold, A.; Dorn, A.; Zappe, H.; Risch, P.; Helmer, D.; Kotz, F.; Rapp, B. E. High-Throughput Injection Molding of Transparent Fused Silica Glass. *Science* **2021**, *372* (6538), 182–186. https://doi.org/10.1126/science.abf1537
(24) Pimenta, M. A.; Dresselhaus, G.; Dresselhaus, M. S.; Cançado, L. G.; Jorio, A.; Saito, R. Studying Disorder in Graphite-Based Systems by Raman Spectroscopy. *Phys Chem Chem Phys* **2007**, *9* (11), 1276–1290. https://doi.org/10.1039/B613962K
(25) Yamauchi, S.; Kurimoto, Y. Raman Spectroscopic Study on Pyrolyzed Wood and Bark of Japanese Cedar: Temperature Dependence of Raman Parameters. *J. Wood Sci.* **2003**, *49* (3), 235–240. https://doi.org/10.1007/s10086-002-0462-1
(26) Dai, X.; Wu, J.; Qian, Z.; Wang, H.; Jian, J.; Cao, Y.; Rummeli, M. H.; Yi, Q.; Liu, H.; Zou, G. Ultra-Smooth Glassy Graphene Thin Films for Flexible Transparent Circuits. *Sci. Adv.* **2016**.

(27) Sharma, S.; Shyam Kumar, C. N.; Korvink, J. G.; Kübel, C. Evolution of Glassy Carbon Microstructure: In Situ Transmission Electron Microscopy of the Pyrolysis Process. *Sci. Rep.* **2018**, *8* (1), 16282. https://doi.org/10.1038/s41598-018-34644-9
(28) Štefelová, J.; Slovák, V.; Siqueira, G.; Olsson, R. T.; Tingaut, P.; Zimmermann, T.; Sehaqui, H. Drying and Pyrolysis of Cellulose Nanofibers from Wood, Bacteria, and Algae for Char Application in Oil Absorption and Dye Adsorption. *ACS Sustain. Chem. Eng.* **2017**, *5* (3), 2679–2692. https://doi.org/10.1021/acssuschemeng.6b03027
(29) Wan, Y. Y.; Zhu, Y. J.; Jiang, L.; Luo, N. Multi-Temperatures Pyrolysis Gas Chromatography: A Rapid Method to Differentiate Microorganisms. *Microorganisms* **2022**, *10* (12), 2333. https://doi.org/10.3390/microorganisms10122333
(30) Fischer, O.; Lemaire, R.; Bensakhria, A. Thermogravimetric Analysis and Kinetic Modeling of the Pyrolysis of Different Biomass Types by Means of Model-Fitting, Model-Free and Network Modeling Approaches. *J. Therm. Anal. Calorim.* **2024**, *149* (19), 10941–10963. https://doi.org/10.1007/s10973-023-12868-w
(31) Schueller, O. J. A.; Brittain, S. T.; Whitesides, G. M. Fabrication of Glassy Carbon Microstructures by Pyrolysis of Microfabricated Polymeric Precursors. *Adv. Mater.* **1997**, *9* (6), 477–480. https://doi.org/10.1002/adma.19970090604
(32) Devi, M.; Rawat, S.; Sharma, S. A Comprehensive Review of the Pyrolysis Process: From Carbon Nanomaterial Synthesis to Waste Treatment. *Oxf. Open Mater. Sci.* **2020**, *1* (1), itab014. https://doi.org/10.1093/oxfmat/itab014
(33) Leifeld, J. Thermal Stability of Black Carbon Characterised by Oxidative Differential Scanning Calorimetry. *Org. Geochem.* **2007**, *38* (1), 112–127. https://doi.org/10.1016/j.orggeochem.2006.08.004
(34) Bastide d'Izard, M.; Abanades, S. Carbothermal Reduction of Hematite Involving Biogenic Carbon Sourced from CO2. *Chem. Eng. J. Adv.* **2025**, *24*, 100925. https://doi.org/10.1016/j.ceja.2025.100925
(35) Tsaneva, V. N.; Kwapinski, W.; Teng, X.; Glowacki, B. A. Assessment of the Structural Evolution of Carbons from Microwave Plasma Natural Gas Reforming and Biomass Pyrolysis Using Raman Spectroscopy. *Carbon* **2014**, *80*, 617–628. https://doi.org/10.1016/j.carbon.2014.09.005
(36) Rouzaud, J. N.; Oberlin, A.; Beny-Bassez, C. Carbon Films: Structure and Microtexture (Optical and Electron Microscopy, Raman Spectroscopy). *Thin Solid Films* **1983**, *105* (1), 75–96. https://doi.org/10.1016/0040-6090(83)90333-4
(37) Dai, X.; Wu, J.; Qian, Z.; Wang, H.; Jian, J.; Cao, Y.; Rummeli, M. H.; Yi, Q.; Liu, H.; Zou, G. Ultra-Smooth Glassy Graphene Thin Films for Flexible Transparent Circuits. *Sci. Adv.* **2016**, *2* (11), e1601574. https://doi.org/10.1126/sciadv.1601574
(38) Ma, J.-F.; Hou, Y.-N.; Guo, J.; Sharif, H. M. A.; Huang, C.; Zhao, J.; Li, H.; Song, Y.; Lu, C.; Han, Y.; Zhang, Y.; Wang, A.-J. Rational Design of Biogenic PdxAuy Nanoparticles with Enhanced Catalytic Performance for Electrocatalysis and Azo Dyes Degradation. *Environ. Res.* **2022**, *204*, 112086. https://doi.org/10.1016/j.envres.2021.112086
(39) Zhang, Y.; Zhao, Q.; Chen, B. Reduction and Removal of Cr(VI) in Water Using Biosynthesized Palladium Nanoparticles Loaded Shewanella Oneidensis MR-1. *Sci. Total Environ.* **2022**, *805*, 150336. https://doi.org/10.1016/j.scitotenv.2021.150336
(40) Xu, H.; Xiao, Y.; Xu, M.; Cui, H.; Tan, L.; Feng, N.; Liu, X.; Qiu, G.; Dong, H.; Xie, J. Microbial Synthesis of Pd–Pt Alloy Nanoparticles Using *Shewanella Oneidensis* MR-1 with Enhanced Catalytic Activity for Nitrophenol and Azo Dyes Reduction. *Nanotechnology* **2019**, *30* (6), 065607. https://doi.org/10.1088/1361-6528/aaf2a6
(41) Lloyd, J. R. Microbial Reduction of Metals and Radionuclides. *FEMS Microbiol. Rev.* **2003**, *27* (2–3), 411–425. https://doi.org/10.1016/S0168-6445(03)00044-5
(42) Ahmed, E.; Kalathil, S.; Shi, L.; Alharbi, O.; Wang, P. Synthesis of Ultra-Small Platinum, Palladium and Gold Nanoparticles by Shewanella Loihica PV-4 Electrochemically

Active Biofilms and Their Enhanced Catalytic Activities. *J. Saudi Chem. Soc.* **2018**, *22* (8), 919–929. https://doi.org/10.1016/j.jscs.2018.02.002